COBEM 2023 27TH INTERNATIONAL CONGRESS OF MECHANICAL ENGENEERING

ABCM Brazilian Society of Mechanical Sciences and Engineering
27th ABCM International Congress of Mechanical Engineering
December 04-08, 2023, Florianópolis-SC, Brazil

COB-2023-1101
ASSESSMENT OF MODAL BALANCING TECHNIQUE APPLIED TO A ROTATING MACHINE SUPPORTED BY DEEP-GROOVE BALL BEARINGS

Yuri Andrade Dias Martins
Thiago de Paula Sales
Aeronautics Institute of Technology, Pç. Mal. Eduardo Gomes, 50 – Vila das Acácias, São José dos Campos, SP, Brazil
yurimartins@ita.br, tpsales@ita.br

Abstract. *Rotating machines are widely employed in many engineering fields, being vastly explored from power generation to aeronautical mobility with high demands. To fulfill the operational requirements and guarantee certain reliability, it is crucial that a given machine runs with acceptable vibration levels within its specified operating range. However, this condition is not always met due to inherently present mechanical faults which cause malfunctions and may lead to excessive bearing wear, potentially compromising the whole rotating assembly lifetime. For this reason, this paper discusses theoretical and experimental unbalance identification in a laboratory test rig comprised of a flexible shaft and a rigid disk, supported by deep-groove ball bearings, modeled using the finite element method. In possession of a representative model of the rotor system, and experimental data measured from the test rig, an optimization problem is posed and solved to identify unknown unbalance parameters, including magnitude and phase. Verification of the rotating assembly new operating condition in terms of vibration levels is performed by comparing orbit plots, velocity amplitudes at the balancing speed and run-up tests. Results show a great reduction in terms of vibration amplitude comparing unbalanced and balanced cases, motivating the application in more complex rotors.*

Keywords: *balancing, optimization, flexible rotor, fault detection*

1. INTRODUCTION

Rotordynamics plays a vital role in several aspects of modern industries, serving as a foundation for various processes and technological advancements. As the main focus of this topic, rotating machines are crucial in manufacturing, energy generation, transportation, and infrastructure. In these fields, machines power production lines, convert mechanical energy into electrical, and facilitate motion. All the aforementioned roles require safe and smooth operation regarding vibration and noise levels, enhancing the machine's lifespan. These operational conditions can only be achieved through monitoring potential failure modes that could lead to breakdowns and financial losses. This examination enables the implementation of fault detection and improvement techniques to prevent such collapses and avoid expensive downtime. Naturally, to apply such approaches, one needs a reliable model of the machine to accurately predict the dynamic behavior under consideration, and avoid potentially critical operating conditions. In this regard, the finite element method (FEM) is extensively employed to model such machines, as it may handle complex geometries associated with challenging boundary conditions, yielding reasonable results. Given these facts, rotordynamics modeling is a well-established topic in the literature, covered by numerous books (Friswell *et al.*, 2010; Lalanne and Ferraris, 1990; Vance *et al.*, 2010; Childs, 2013; Krämer, 2013; Adams, 2000; Darlow, 2012; Genta, 2007).

A rotating machine can experience various potential faults, such as unbalance, misalignment, shaft bow, bearing wear, shaft cracks, as well as gear defects. Each of these faults requires a specific approach for identification and correction. However, these issues can occur simultaneously, posing a greater challenge in managing the situation, since some may exhibit similar vibration signatures in time and frequency domains (Lal and Tiwari, 2012). Despite long-standing research on some of these faults, unbalance remains the most extensively studied, as it represents one of the primary causes of lateral vibrations in rotors. The forces generated by eccentricity are present in virtually all rotating machines, regardless of efforts to minimize them. Machine assembly and geometric imperfections due to manufacturing process inherently introduce a certain level of unbalance in rotors, which can lead to undesired lateral vibrations and, consequently, bearing wear and failures (Swanson *et al.*, 2005; Sanches and Pederiva, 2016).

Recent research on balancing techniques has focused on reducing the number of trial runs and measurement points, eliminating the need for trial weights, and optimizing the selection of balancing planes, as advancements in balancing techniques continue. The importance of balance lies in its ability to counteract the adverse effects of unbalance forces and moments that arise during operation. An unbalanced rotor may experience high levels of stresses in critical components, which will eventually fail. These undesired vibrations can be minimized by systematically balancing the machine, ensuring smoother operation and optimizing performance, thus mitigating detrimental effects (Li *et al.*, 2021; Ibraheem *et al.*, 2019).

In the field of rotor balancing, there are two traditional and well-established approaches: the influence coefficient method (ICM) and the modal balancing method (MBM).

The ICM, originally proposed by Thearle (1934), has demonstrated its practicality in balancing field rotors without relying on a model. Its effectiveness lies in the ability to accurately determine the influence coefficient matrix, allowing precise balancing calculations and adjustments. This aspect represents one of the main advantages of the ICM over the MBM, as the latter requires prior knowledge of the machine, i.e., the mode shapes information. It is also worth emphasizing that in the ICM approach, several trial runs are performed at a single rotational speed, with correction masses being applied independently for each trial.

In contrast, the MBM focuses on balancing the rotor near each critical speed of interest, where the corresponding mode shape is dominant, and aims to mitigate the influence of each mode in the rotor's response, rather than reducing the amplitude response to zero (Friswell *et al.*, 2010; Li *et al.*, 2021). One of the pioneering studies on what was commonly referred to as modal balancing was conducted by Bishop and Gladwell (1959). In their research, an unbalanced flexible rotor underwent the MBM process mode by mode to achieve the balanced condition.

In this regard, Morais *et al.* (2014) investigated an optimization procedure related to unbalance distribution in a rotating machine with localized nonlinearity using pseudo-random algorithms. The main goal was to propose a methodology to overcome the most common limitations regarding the conventional balancing techniques, e.g., several trial runs, time consumption, linear behavior assumption. At first, a reliable model of the rotating machine was identified through model updating. Subsequently, the unbalance distribution in a linear case was identified, without the need for trial runs. An electromagnetic actuator (EMA) located at the bearing position provided the system's nonlinearity. The updated model accurately represented the experimental test rig behavior in the range of the first two vibration modes. Consequently, the unbalance distribution was successfully identified, and the amplitudes related to the first critical speed were significantly reduced for both linear and nonlinear cases. Thus, the proposed method overcomes the ICM by enabling the rotor to be balanced in a single run-up or run-down, albeit requiring a reliable model.

Saldarriaga *et al.* (2010) proposed a methodology for balancing a very flexible rotating machine by solving an inverse problem. The research is mainly focused on providing insight into rotor balancing when conventional techniques, e.g., MBM, cannot be applied due to high vibration amplitudes. The experimental test rig comprised a flexible shaft and three different disks supported by roller bearings. At first, the bearings' parameters were identified using an optimization procedure, taking into account experimental and theoretical frequency response functions (FRFs), where FEM provided the latter. In the sequence, the unbalance identification was performed using genetic algorithms, setting the objective function as the squared difference of calculated and measured accelerations, with design variables chosen as magnitude and phase of unbalance. The estimated FRFs using the identified bearings' parameters provided satisfactory results. Furthermore, the displacement amplitude at the rotating frequency was greatly reduced after positioning correction masses. In summary, results were convincing, considering that the machine experienced large displacements due to its highly flexible condition.

A summary of other researches which have been performed, relevant to this work, is now provided. First, Yao *et al.* (2018) presented a method for identifying and optimizing unbalance parameters in rotor-bearing systems. The method utilized a modal expansion approach combined with optimization algorithms, successfully reducing vibration amplitudes by accurately locating and correcting the unbalance through simulations and experiments. On the other end, Sanches and Pederiva (2016) discussed the simultaneous identification of unbalance and residual shaft bow in the time domain. Given their synchronous nature with rotation, separating their effects posed challenges. However, employing a correlation analysis procedure consistently identified these faults in a Laval experimental test rig. Cruz *et al.* (2019) performed modeling and experimental validation of vibration characteristics under unbalance conditions of a multi-stage rotor. The main goal was to investigate the effects induced by a known unbalance mass added to the stage disks, and how the critical speeds would change according to the unbalance magnitude, phase and position along the shaft. Sudhakar and Sekhar (2011) investigated a procedure of unbalance identification in a rotor-bearing system. A model-based method was implemented, minimizing the equivalent loads between the experimental measures and theoretical predictions. Results were consistent in identifying the location and severity of the unbalance. Deepthikumar *et al.* (2013) studied the procedure of modal balancing in the presence of shaft bow. The method was based on a polynomial curve for eccentricity distribution to identify the distributed unbalance along the shaft. The rotor safely passed through the first critical speed after the mass correction. Quinz *et al.* (2021) proposed the Numerical Assembly Technique (NAT) to achieve balance of a linear elastic rotor-bearing system with arbitrarily distributed unbalance. Investigations have shown that NAT is a powerful tool because it can provide quasi-analytical solutions, making it more computationally efficient than FEM. Using the traditional MBM, the rotors were systematically balanced in three different test cases, yielding convincing results even in the case of distributed unbalance, significantly reducing amplitudes at the first three critical speeds. Finally, Sun *et al.* (2022) investigated a balancing method for multi-disk flexible rotors without the need for trial weights. The procedure is based on the traditional MBM, which approximates the original unbalance distribution as isolated unbalances acting on the balancing planes, specifically the disks. This method demonstrates robustness in handling anisotropic bearings and multiple disks, as evidenced by several test cases. Results after low- and high-speed balancing show a significant reduction in the orbit's amplitude.

Considering the previous exposition, in the present study, our primary objective is to perform the balance of a single-disk flexible rotating machine supported by deep-groove ball bearings, depicted in Fig. 1, using a modal balancing technique.

To obtain good representation of the system, FEM models were adjusted taking into account individual component characterizations, using experimental frequency response measurements. The balancing procedure was then executed, by utilizing modal information associated with the first planar vibration mode, adopting the disk as balancing plane. Experimental measurements were conducted as trial runs, to compute unbalance magnitude and phase corrections, aiming to eliminate the influence of the first bending mode on the system's dynamic response. Afterward, we compare results in terms of orbit plots and frequency domain amplitudes, both before and after the balancing procedure, emphasizing crucial aspects related to unbalance magnitude and phase. This comprehensive approach seeks to provide valuable insights into the effectiveness of the modal balancing technique, and its impact on the overall dynamics of the machine, which seems to show some nonlinear behavior.

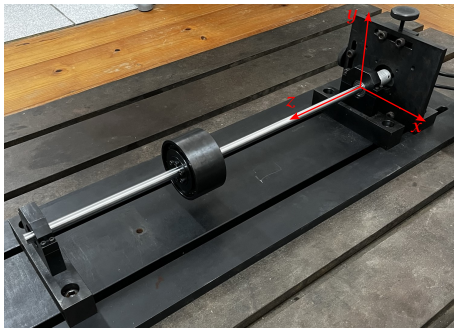

Figure 1: Single-disk flexible rotating machine supported by deep-groove ball bearings.

In addition to this introduction, this work is divided into five additional sections, each addressing specific aspects of the study. Section 2 is dedicated to mathematical modeling, where the theoretical framework and equations describing the system are presented in detail. Section 3 comprises the description of the experimental test rig, and operating conditions. Section 4 focuses on the presentation and discussion of numerical and experimental results. Both simulation data and measurements are analyzed, allowing for a comprehensive evaluation of the system's behavior, providing valuable insights into the performance of the proposed approach. Main conclusions drawn from the study are presented in Section 5, highlighting the key findings. Acknowledgments and references come afterward.

2. MATHEMATICAL MODELING

2.1. Rotor system model

In general, rotating machines are widely modeled as beam finite elements, accounting for the spinning forces arising from rotation about the longitudinal axis. The mathematical model of the rotor depicted in Fig. 1 is based on Timoshenko's beam theory, which accounts for the shear deformation of the cross-section. The disks are assumed to be rigid and are modeled as point masses and inertia added to their respective degrees of freedom (DoF). Furthermore, the dynamic effects caused by the bearings are addressed by presuming a linear load-deflection relationship between the forces acting on the shaft and the resulting displacements and velocities. Although the assumed linear model for the bearings is widely used, some research has shown the importance of considering nonlinear behavior to improve predictions (Harsha, 2005, 2006; Sharma *et al.*, 2018; Changqing and Qingyu, 2006; Thibault *et al.*, 2022).

Considering that the rotor experiences small displacements, the rotating linear time-invariant system's equation of motion (EoM) is given in general form:

$$\mathbf{M}\ddot{\mathbf{q}} + (\mathbf{C} + \Omega\mathbf{G})\dot{\mathbf{q}} + \mathbf{K}\mathbf{q} = \mathbf{Q}, \tag{1}$$

where $\mathbf{M}$, $\mathbf{C}$, $\mathbf{G}$ and $\mathbf{K}$ represent the mass, general damping, gyroscopic and stiffness matrices, respectively; $\ddot{\mathbf{q}}$, $\dot{\mathbf{q}}$, $\mathbf{q}$ and $\mathbf{Q}$ account for generalized accelerations, velocities, displacements and loads, respectively; Ω express the rotor rotational speed. The vector $\mathbf{q}$ and its respective time derivatives contain the translations and rotations DoF associated with the Timoshenko's beam theory. The previously mentioned matrices are well-established and covered by Friswell *et al.* (2010), Lalanne and Ferraris (1990) and Nelson (1980). Regarding the modeling of the bearings and the flexible coupling, the stiffness contributions due to these components can be suitably incorporated into matrix $\mathbf{K}$, using:

$$\mathbf{K}_b = \begin{bmatrix} k_{u,b} & 0 & 0 & 0 \\ 0 & k_{v,b} & 0 & 0 \\ 0 & 0 & k_{\theta,b} & 0 \\ 0 & 0 & 0 & k_{\psi,b} \end{bmatrix}, \quad \mathbf{K}_c = \begin{bmatrix} 0 & 0 & 0 & 0 \\ 0 & 0 & 0 & 0 \\ 0 & 0 & k_{\theta,c} & 0 \\ 0 & 0 & 0 & k_{\psi,c} \end{bmatrix}, \tag{2}$$

where $k_{u,b}$ and $k_{v,b}$ accounts for bearing translational stiffness in x and y directions (cf. Fig. 1), whereas $k_{\theta,b}$ and $k_{\psi,b}$ are related to rotational stiffness around y and x, respectively. Analogously, $k_{\theta,c}$ and $k_{\psi,c}$ refer to the coupling rotational stiffness around the same directions.

2.2. Unbalance modeling

Considering the difference between the equilibrium position and the center of mass of the rotor is given by $\mathbf{q}_\epsilon$ and substituting $\mathbf{q}$ by $(\mathbf{q}+\mathbf{q}_\epsilon)$ in the inertia and gyroscopic terms of Eq. (1), neglecting external forces, one may reach (Friswell *et al.*, 2010; Darlow, 2012; Vance *et al.*, 2010):

$$\mathbf{M}\left(\ddot{\mathbf{q}}+\ddot{\mathbf{q}}_\epsilon\right)+\Omega\mathbf{G}\left(\dot{\mathbf{q}}+\dot{\mathbf{q}}_\epsilon\right)+\mathbf{C}\dot{\mathbf{q}}+\mathbf{K}\mathbf{q}=\mathbf{0}. \tag{3}$$

Exploring harmonic excitation characteristics, one may use $\dot{\mathbf{q}}_\epsilon = j\Omega\mathbf{q}_\epsilon$ and $\ddot{\mathbf{q}}_\epsilon = -\Omega^2\mathbf{q}_\epsilon$:

$$\mathbf{M}\ddot{\mathbf{q}}+(\mathbf{C}+\Omega\mathbf{G})\,\dot{\mathbf{q}}+\mathbf{K}\mathbf{q}=\Omega^2\mathbf{M}\mathbf{q}_\epsilon-j\Omega^2\mathbf{G}\mathbf{q}_\epsilon. \tag{4}$$

Also, assuming the unbalance is placed at a particular node n of the FE model, the corresponding vector related to the disk element is given by:

$$\mathbf{q}_n=\mathrm{Re}\left\{\begin{Bmatrix}\epsilon\mathrm{e}^{\mathrm{j}\delta}\\-\mathrm{j}\epsilon\mathrm{e}^{\mathrm{j}\delta}\\\mathrm{j}\beta\mathrm{e}^{\mathrm{j}\gamma}\\\beta\mathrm{e}^{\mathrm{j}\gamma}\end{Bmatrix}\mathrm{e}^{\mathrm{j}\Omega t}\right\},\qquad \text{with } \mathrm{j}=\sqrt{-1}. \tag{5}$$

where ϵ denotes the offset distance at the disk, β corresponds to an offset angle, and δ and γ refer to the unbalance forces and moment phase angles, respectively. Substituting Eq. (5) into the right-hand side of Eq. (4), one reaches:

$$\Omega^2\mathbf{M}_{n,d}\mathbf{q}_\epsilon-j\Omega^2\mathbf{G}_{n,d}\mathbf{q}_\epsilon=\mathrm{Re}\left\{\Omega^2\begin{Bmatrix}m_n\epsilon\mathrm{e}^{\mathrm{j}\delta}\\-\mathrm{j}m_n\epsilon\mathrm{e}^{\mathrm{j}\delta}\\\mathrm{j}(I_{d,n}-I_{p,n})\beta\mathrm{e}^{\mathrm{j}\gamma}\\(I_{d,n}-I_{p,n})\beta\mathrm{e}^{\mathrm{j}\gamma}\end{Bmatrix}\mathrm{e}^{\mathrm{j}\Omega t}\right\}=\mathrm{Re}\left\{\,\Omega^2\mathbf{b}_0\mathrm{e}^{\mathrm{j}\Omega t}\,\right\}. \tag{6}$$

where $\mathbf{M}_{n,d}$ and $\mathbf{G}_{n,d}$ denotes the element mass and gyroscopic matrices of a disk at the n-th node. In Eq. (6), the component $\Omega^2\mathbf{b}_0$ denotes the unbalance vector that acts at the same node. In this way, one may write:

$$\mathbf{M}\ddot{\mathbf{q}}+(\mathbf{C}+\Omega\mathbf{G})\,\dot{\mathbf{q}}+\mathbf{K}\mathbf{q}=\mathrm{Re}\left\{\,\Omega^2\mathbf{b}_0\mathrm{e}^{\mathrm{j}\Omega t}\,\right\}. \tag{7}$$

Solving Eq. (7) by assuming harmonic response as $\mathbf{q}=\mathrm{Re}\left\{\,\mathbf{q}_0\mathrm{e}^{\mathrm{j}\Omega t}\,\right\}$, gives:

$$\mathbf{q}_0=\left[(\mathbf{K}-\Omega^2\mathbf{M})+\mathrm{j}\Omega(\mathbf{C}+\Omega\mathbf{G})\right]^{-1}\Omega^2\mathbf{b}_0. \tag{8}$$

2.3. Modal balancing method

As stated before, the MBM aims to establish a systematic procedure to annihilate the influence of each mode amplification factor in the dynamic response of the machine, one by one. Naturally, the procedure begins by addressing the balancing of the lower modes, ensuring that the operational conditions are sufficiently secure to run the machine through critical speeds associated with the balanced modes. Assuming that $\mathbf{b}$ is a vector containing the total unbalance distribution on the rotor, i.e., the sum of inherent unbalance and corrections applied by MBM, it can be decomposed as (Friswell *et al.*, 2010; Adams, 2000; Darlow, 2012):

$$\mathbf{b}=\mathbf{b}_0+\mathbf{b}_c, \tag{9}$$

where $\mathbf{b}_0$ is the same of Eq. (8), and $\mathbf{b}_c$ accounts for the total correction, given by the sum of modal contributions:

$$\mathbf{b}_c=\sum\nolimits_{k=1}^{m}\mathbf{b}_{c,k}, \tag{10}$$

where m represents the highest mode to be balanced, and $\mathbf{b}_{c,k}$ the correction associated with k-th mode. In this context, to ensure the effectiveness of modal balancing, it is essential that:

$$\mathbf{u}_k^{\mathsf{T}}\mathbf{b}=0, \tag{11}$$

where $\mathbf{u}_k$ denotes the k-th mode shape.

The balancing corrections shown in Eq. (10) may be written in terms of:

$$\mathbf{b}_{c,k} = \alpha_k \mathbf{e}_k, \tag{12}$$

where $\mathbf{e}_k$ denotes a basis vector and α_k is a complex scalar. The basis vector must satisfy the orthogonality properties:

$$\mathbf{u}_k^{\mathsf{T}} \mathbf{e}_k = 1, \qquad \text{and} \qquad \mathbf{u}_j^{\mathsf{T}} \mathbf{e}_k = 0 \qquad \text{for all } j < k. \tag{13}$$

In an attempt to balance an arbitrary mode k, one must consider $\alpha_k = 0$ in the first run so that only the components of $\mathbf{b}_{0,k}$ due to the current mode are present in $\mathbf{b}$, as stated by Eq. (9). Measuring the response of the rotor close to the critical speed in this condition gives the necessary information about the inherent unbalance distribution. Subsequently, a trial balance $\mathbf{b}_{t,k} = \delta_k \mathbf{e}_k$ is added at the balancing plane, where δ_k corresponds to a positive real scalar. One may compute the difference between the two measurements as $\mathbf{r}_{d,k} = \mathbf{r}_k - \mathbf{r}_{0,k}$ to effectively calibrate the corrective balance. Naturally, these responses are experimental quantities, but they are theoretically given by Eq. (8), considering $\mathbf{b}_0$ properly. In possession of the measurements, one may compute α_k as:

$$\alpha_k = -\delta_k \left(\mathbf{r}_{d,k}^{\mathsf{H}} \mathbf{r}_{0,k} \right) \Big/ \left(\mathbf{r}_{d,k}^{\mathsf{H}} \mathbf{r}_{d,k} \right), \tag{14}$$

where $^{\mathsf{H}}$ denotes the Hermitian transpose. The first mode corrective balance is calculated through Eq. (12) to guarantee the condition established in Eq. (11). The effect of applying α_k to the initial trial balance is to obtain a condition where the correction magnitude and phase are opposite to the inherent condition, providing a systematically balanced machine. Other modes may be addressed following the same procedure listed above.

2.4. Optimization procedure

In practical implementation, the corrective balance must be converted into tangible quantities for application on the rotor. The balancing plane, illustrated schematically in Fig. 2, comprise a disk with 24 evenly spaced holes. These holes are utilized for inserting screws and washers based on the information provided in vector $\mathbf{b}_c$. It is important to note that there are limitations on the permissible magnitude and phase adjustments during the correction process due to the radial spacing of the holes, $\phi = 15°$, and mass adjustment using a combination of screws and washers within each hole. An optimization procedure was adopted to determine the optimal configuration of screws and washers to be applied on the balancing plane based on the magnitude and phase of the corrective vector. The Genetic Algorithm was employed to minimize the discrepancy between the calculated corrective vector and a vector that accurately replicates the desired configuration.

In this regard, the objective function $\mathbf{F}(\mathbf{X})$ may be written as:

$$\mathbf{F}(\mathbf{X}) = \|\mathbf{b}_c - \mathbf{b}_e(\mathbf{X})\| \big/ \|\mathbf{b}_c\|, \tag{15}$$

where $\mathbf{b}_c$ comes from the modal balancing procedure and $\mathbf{b}_e(\mathbf{X})$ represents the equivalent balance configuration to be applied in the rotor, depending on the design variables' vector $\mathbf{X}$. $\mathbf{b}_e$ is calculated using:

$$\mathbf{b}_e(\mathbf{X}) = \sum_{i=1}^{n} m_{e,i}(\mathbf{X})\, \mathbf{r}_{e,i} = \sum_{i=1}^{n} m_{e,i}(\mathbf{X})\, r_h \begin{Bmatrix} \cos\theta_{s,i} \\ \sin\theta_{s,i} \end{Bmatrix}, \tag{16}$$

where n is the number of holes, r_h represents the radius of the holes' circle, and $\theta_{s,i}$ refers to the angular position of each hole. The corrective mass $m_{e,i}(\mathbf{X})$ for a specific hole is stated as:

$$m_{e,i}(\mathbf{X}) = n_{s,i}(m_s + n_{w,i} m_w), \tag{17}$$

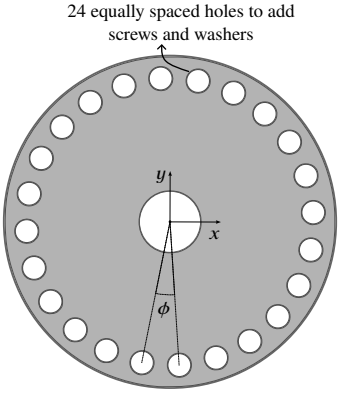

Figure 2: Schematic representation of rigid disk, highlighting tapped holes used to add corrective balance.

where $n_{s,i}$ is a Boolean operator to add or not a screw at hole i, $n_{w,i}$ is a positive scalar related to the number of washers installed at hole i, and m_s and m_w are the screw and washer masses, respectively.

In the adopted optimization procedure, the design variables vector $\mathbf{X}$ collects $n_{s,i}$ and $n_{w,i}$, for all holes, therefore leading to 48 (integer) unknowns. In the optimization problem resolution, one has considered appropriate constraints and bounds for the design variables, to avoid spurious, unrealistic solutions.

3. EXPERIMENTAL TEST RIG

The experimental test rig depicted in Fig. 3a consists of a flexible shaft with a rigid disk supported by deep-groove ball bearings. It features a 15 mm diameter steel shaft with a total length of 700 mm. The rigid disk, positioned at 435 mm from the left bearing, is made of steel, has an external diameter of 100 mm, thickness of 55 mm, and has mass approximately equal to 3 kg. The shaft is supported by a pair of deep-groove ball bearings, mounted on a 20 mm bearing housing. A flexible coupling connects the rotor shaft and the driving motor. The electric motor nominal operating speed range is between 0–6000 rpm. In this setup, the experimental measurements were obtained using a laser doppler vibrometer positioned at the disk, capturing both rotating and non-rotating vibration amplitudes.

An optimization procedure was conducted to adjust the values of the shaft material Young's modulus, bearing and coupling stiffness, as they were not accurately known. A model updating technique was employed, minimizing the disparity between the theoretical and experimental FRFs under non-rotating conditions, following the methodology outlined by Sanches and Pederiva (2016) and Junior (2013). The updated values resulted in a more accurate representation of the experimental test bench, providing a reliable model.

In terms of FE modeling, Fig. 3b depicts the mesh consisting of 61 Timoshenko shaft-beam elements, a rigid disk and a pair of bearings modeled using springs and dampers at each end. Additionally, a highlighted region is shown representing the disk interface modeling, where the diameter of the shaft was increased in the disk region to accurately capture the localized stiffness increase resulting from the experimental attachment.

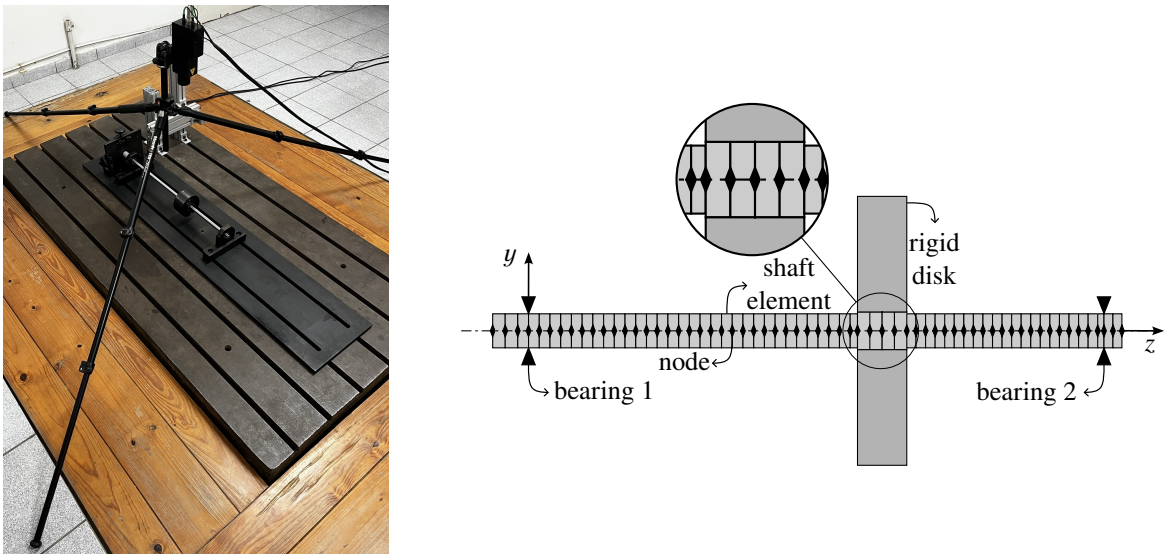

(a) Experimental setup with laser sensor

(b) One dimensional FE model of the experimental test rig

Figure 3: Experimental test rig with sensor positioned to measure at disk, and its discretized model.

4. RESULTS AND DISCUSSION

4.1. FE model adjustment

The FE model was updated using driving points FRFs at the disk location. Measurements were taken in x and y directions, in order to update unknown parameters related to the bearings' and coupling stiffness, Eq. (2), and shaft Young's modulus. Figure 4 shows results in terms of mobility, for the frequency range of interest, i.e., 0–300 Hz.

As can be observed, the updated model tracks well the experimental curve within the region of interest. The first vibration mode in both FRFs is nicely represented by the FE model, whereas a slight frequency shift can be seen near the second resonance. Nevertheless, the modal information needed for the balancing technique, in our case, lies on the first mode, which is properly reproduced by FEM. Furthermore, as the natural frequencies related to the first two modes are almost the same in both directions, one may conclude that the system is practically isotropic.

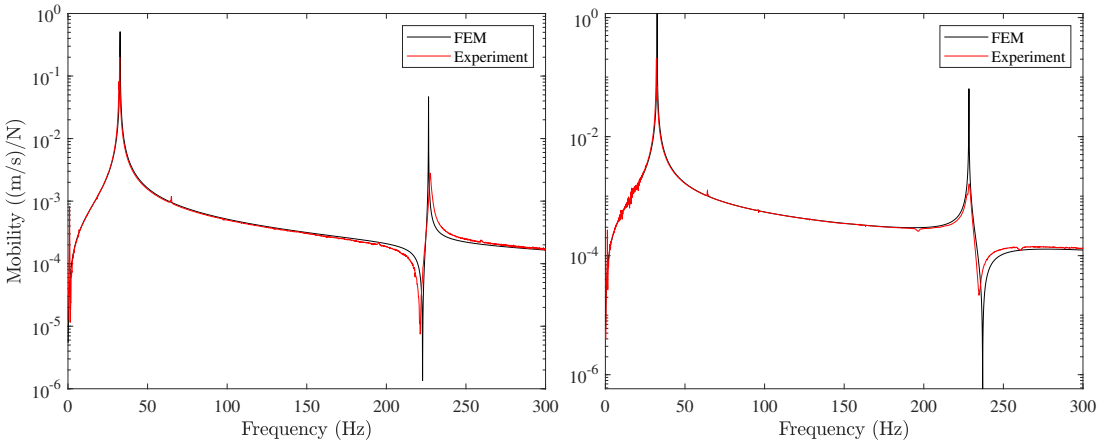

(a) Horizontal direction (b) Vertical direction

Figure 4: Mobility FRFs used for FE model updating, and resulting model predictions.

4.2. Balanced configuration

In possession of a reliable model, the first critical speed was estimated from the Campbell's diagram (not shown here due to length limitation) as 1922 rpm. Accordingly, the experimental measurements were taken at a safe operational speed of 1730 rpm, i.e., approximately 90 % of the predicted value.

Initially, the machine was set to operate at the desired speed without any masses added to the balancing planes, in order to obtain the influence of the inherent unbalance $\mathbf{r}_{0,1}$ in the vertical direction. Subsequently, a configuration of screws and washers was determined, by considering the minimization of Eq. (15), using modal information, to properly calibrate the model, and obtain $\mathbf{r}_1$. Following these measurements, $\mathbf{r}_{d,1} = \mathbf{r}_1 - \mathbf{r}_{0,1}$ was calculated to obtain the influence of the calibrating mass, only. Then, the first correction balance was computed, by evaluating α_1 in Eq. (14). This process was repeated three times until convergence, resulting in the balanced configuration shown in Fig. 5, where balance correction corresponds to 318.11 g mm at 182.6°.

Looking at the distribution of screws and washers, it can be observed that the added mass ranges from a screw plus 1 washer, to a screw plus 8 washers. It is important to highlight that the maximum number of washers per hole was limited to 9, to ensure that the mass was added within the balancing plane and not outside of it. Referring to Fig. 3a, we can see that the system involves a thick disk with two balancing planes, one on each side. The balancing plane nearest to the center of the shaft was selected due to the higher vibration amplitudes observed in that location.

To effectively compare the unbalanced and balanced configurations, Fig. 6 presents orbit plots, filtered at the balancing speed, before and after the procedure employed in this research, along with velocity amplitude and phase in the frequency domain for vertical measurements.

As shown in Fig. 6a, the velocity amplitude reduction at the balancing plane was nearly ten times from the unbalanced to the balanced configuration, demonstrating the effectiveness of the proposed method in mitigating undesired vibrations caused by unbalance faults. Furthermore, by posing an optimization procedure considering the difference between theoretical and experimental unbalanced orbits, it was possible to identify the magnitude and phase that reproduces the experimental condition theoretically, which is shown in the black solid curve. Although the phase was not accurately

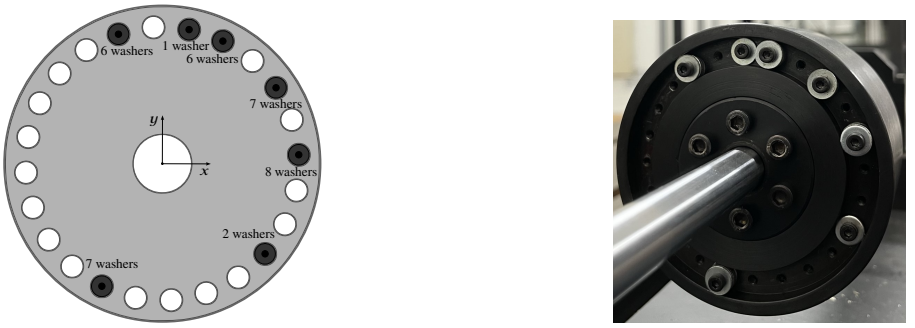

(a) Schematic representation of the disk with corrections (b) Photograph of the disk with installed corrections

Figure 5: Distribution of correction masses used to balance the first mode of the experimental test rig.

predicted, as the black ellipse is slightly rotated with respect to the red one, the magnitude was reasonably estimated by FEM. Additionally, Fig. 6b displays the amplitude of the orbit in the frequency domain, revealing that the vector's phase is closely aligned with the orbit's semi-major axes.

Moreover, it can be observed in Fig. 7, in the frequency domain, a great amplitude reduction at the 1X rotational frequency chosen to perform balance (1730 rpm). Between 30–40 Hz, some peaks may be identified in both experimental velocities, and are related to the first critical speed. Also, Fig. 7a shows a slightly smaller amplitude for the balanced case, compared to the result in Fig. 7b, reinforcing the quasi-circular orbit seen in Fig. 6a. In terms of reduction, Tab. 1 shows both unbalanced and balanced velocity amplitudes at the balancing speed. As can be noted, the amplitude reduction at 1X peaks was as high as 91.43% horizontally, which represents a massive vibration decrease.

Table 1: Vibration amplitude comparison at the balancing speed, before and after performing MBM.

Direction	**Balanced** (m/s)	**Unbalanced** (m/s)	**Reduction** (%)
Horizontal	0.0012	0.0141	91.4290
Vertical	0.0020	0.0142	85.6960

One of the many ways to verify the effectiveness of balancing consists in run the machine through a critical speed, after the corresponding mode has been balanced. In this regard, Fig. 8 depicts a run-up of both balanced and unbalanced cases. From Fig. 8b, one can observe that, in the balanced case, the machine runs up to 2300 rpm, whereas the same speed cannot be reached in the unbalanced condition, due to the possibility of a breakdown. In this way, the run-up is performed until 1900 rpm for the red curve. Both accelerations were synchronized to better compare the effects of balancing. It can be observed from Fig. 8a that until 10 s, the velocity amplitudes are quite equal for both cases. Between 10–20 s, the unbalanced case exhibits slightly higher amplitudes. Additionally, both curves show a peak amplitude at approximately

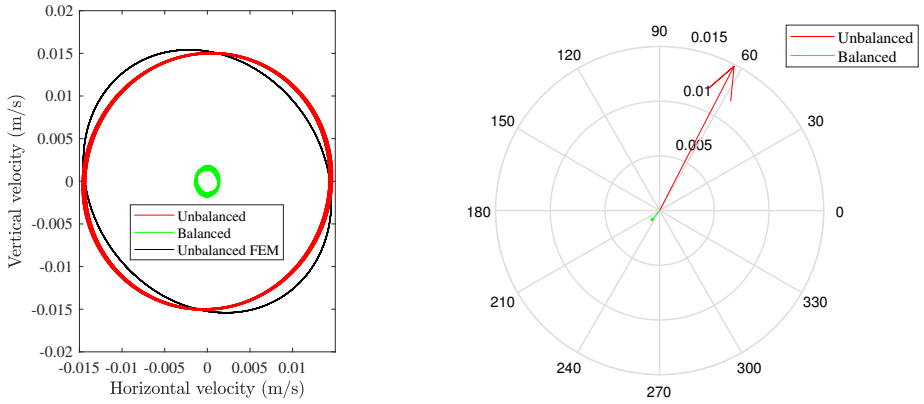

(a) Velocity orbits

(b) Velocity amplitude and phase polar plot

Figure 6: Comparison of unbalanced and balanced responses at the balancing speed (1730 rpm).

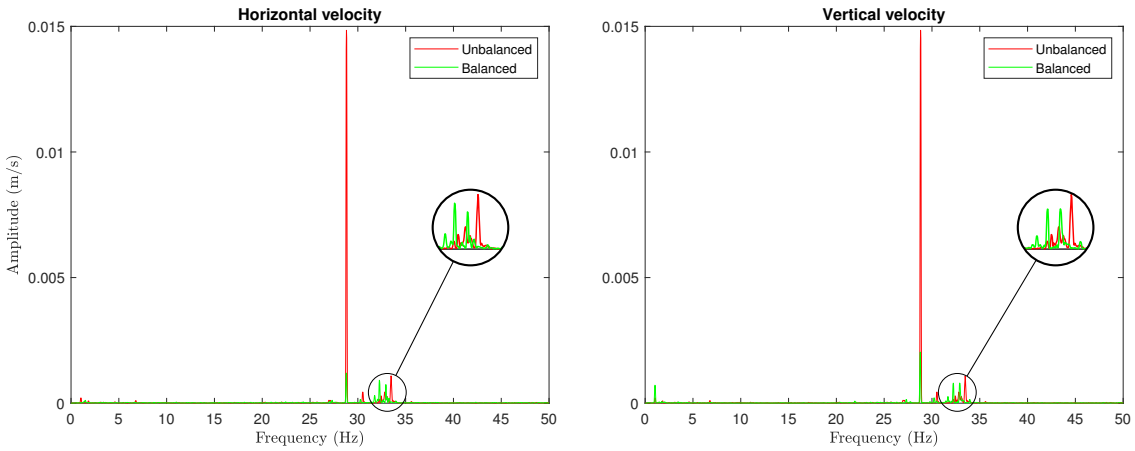

(a) Horizontal velocity frequency spectrum

(b) Vertical velocity frequency spectrum

Figure 7: Frequency spectra of velocity signals measured before and after balancing of the test rig, operating at 1730 rpm.

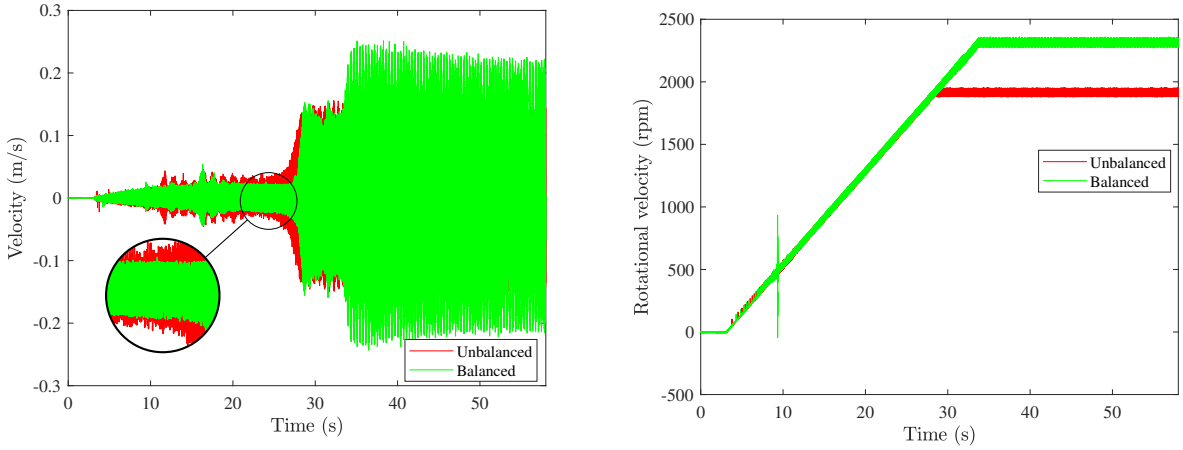

(a) Vertical velocities measured at the disk location

(b) Histories of the shaft rotational speed

Figure 8: Experimental measurements obtained by performing a run-up procedure.

16 s, attributed to a nonlinear phenomenon known as ball spin frequency (BSF) (Friswell *et al.*, 2010). By calculating the oscillation period and frequency at 16 s, the approximate value is found to be 33 Hz, while the rotational frequency at the same time is around 16 Hz, indicating the presence of a 2X phenomenon.

Focusing on the time interval of 20–30 s, the zoomed region highlights the balancing procedure's effectiveness, as the balancing speed (1730 rpm) lies within this interval. Actually, the amplitude reduction is greater than shown in the run-up, since both curves do not reach a stationary regime in this case, with transient effects always present. After 30 s, the velocity amplitude grows considerably due to the machine reaching its first critical speed. At this point, the unbalanced rotor no longer accelerates, while the balanced system continues to increase its rotational speed. Although a decrease in amplitude was expected after the first critical speed, the green curve reaches even larger values. This phenomenon might be attributed to a discrepancy between the predicted and actual critical speed values, resulting in a lower balancing speed compared to the experimental conditions. As a result, effects of the first vibration mode were not adequately mitigated.

5. CONCLUDING REMARKS

In this paper, an investigation of field modal balancing applied to a single-disk rotating machine with deep-groove ball bearings has been considered. The system was modeled using FEM to numerically compute FRFs, modal information, and predictions associated with critical speeds, in order to perform the desired approach. Naturally, modeling complex systems always gives rise to inherent uncertainties related to boundary conditions and material properties that need to be updated in order to better represent experimental conditions. In this regard, a model updating technique was applied to minimize the discrepancy between theoretical and experimental data, resulting in reliable predictions for the first critical speed, purportedly. Subsequently, the balancing technique was executed by running the machine at the selected balancing speed, and by adding correction masses until convergence. The calculated correction masses enabled a significant reduction in the measured quantities, resulting in a quasi-circular orbit for the balanced configuration filtered at the balancing speed. Frequency response plots were also compared, highlighting the significant reduction in amplitude at the 1X rotational frequency. Furthermore, a run-up comparison evidenced the presence of a nonlinear phenomenon related to the bearings and some discrepancies between expected and actual results, albeit an amplitude reduction was observed near the balancing speed. Further investigations are to be performed by the authors to better understand the system analyzed in this paper.

6. ACKNOWLEDGMENTS

Y. A. D. Martins acknowledges his master scholarship by the Brazilian National Council for Scientific and Technological Development (CNPq). T. P. Sales is grateful to the São Paulo Research Foundation (FAPESP) for its support to the thematic grant #18/15894-0, related to the "Periodic structure design and optimization for enhanced vibroacoustic performance: ENVIBRO" research project; and to the Brazilian Coordination for the Improvement of Higher Education Personnel (CAPES).

7. REFERENCES

Adams, M., 2000. *Rotating Machinery Vibration: From Analysis to Troubleshooting*. EBSCO ebook academic collection. Taylor & Francis. ISBN 9780824745417.

Bishop, R.E.D. and Gladwell, G.M.L., 1959. "The vibration and balancing of an unbalanced flexible rotor". *Journal of Mechanical Engineering Science*, Vol. 1, No. 1, pp. 66–77.

Changqing, B. and Qingyu, X., 2006. "Dynamic model of ball bearings with internal clearance and waviness". *Journal of Sound and Vibration*, Vol. 294, No. 1, pp. 23–48. ISSN 0022-460X.

Childs, D., 2013. *Turbomachinery Rotordynamics with Case Studies*. Minter Spring. ISBN 9780615852720.

Cruz, W., Arzola, N. and Araque, O., 2019. "Modeling and experimental validation of the vibration in an unbalance multi-stage rotor". *Journal of Mechanical Engineering and Sciences*, Vol. 13, No. 3, pp. 5703–5716.

Darlow, M., 2012. *Balancing of High-Speed Machinery*. Mechanical Engineering Series. Springer New York. ISBN 9781461236566.

Deepthikumar, M., Sekhar, A. and Srikanthan, M., 2013. "Modal balancing of flexible rotors with bow and distributed unbalance". *Journal of Sound and Vibration*, Vol. 332, No. 24, pp. 6216–6233. ISSN 0022-460X.

Friswell, M., Penny, J., Lees, A. and Garvey, S., 2010. *Dynamics of Rotating Machines*. Cambridge University Press.

Genta, G., 2007. *Dynamics of Rotating Systems*. Mechanical Engineering Series. Springer New York. ISBN 9780387286877.

Harsha, S., 2005. "Nonlinear dynamic analysis of an unbalanced rotor supported by roller bearing". *Chaos, Solitons and Fractals*, Vol. 26, No. 1, pp. 47–66. ISSN 0960-0779.

Harsha, S., 2006. "Nonlinear dynamic response of a balanced rotor supported by rolling element bearings due to radial internal clearance effect". *Mechanism and Machine Theory*, Vol. 41, No. 6, pp. 688–706. ISSN 0094-114X.

Ibraheem, A.A., Ghazaly, N.M. and Jaber, G.T.A.e., 2019. "Review of rotor balancing techniques". *American Journal of Industrial Engineering*, Vol. 6, No. 1, pp. 19–25. ISSN 2377-4339.

Junior, A.A.C., 2013. *Detection and identification of incipient transversal cracks in flexible and horizontal shafts of rotating machines*. Ph.D. thesis, Graduate Program in Mechanical Engineering, Federal University of Uberlandia, Uberlandia, Brasil.

Krämer, E., 2013. *Dynamics of Rotors and Foundations*. Springer Berlin Heidelberg. ISBN 9783662027981.

Lal, M. and Tiwari, R., 2012. "Multi-fault identification in simple rotor-bearing-coupling systems based on forced response measurements". *Mechanism and Machine Theory*, Vol. 51, pp. 87–109. ISSN 0094-114X.

Lalanne, M. and Ferraris, G., 1990. *Rotordynamics prediction in engineering*. Wiley.

Li, L., Cao, S., Li, J., Nie, R. and Hou, L., 2021. "Review of rotor balancing methods". *Machines*, Vol. 9, No. 5, p. 89.

Morais, T., Der Hagopian, J., Steffen, V. and Mahfoud, J., 2014. "Optimization of unbalance distribution in rotating machinery with localized non linearity". *Mechanism and Machine Theory*, Vol. 72, pp. 60–70. ISSN 0094-114X.

Nelson, H.D., 1980. "A finite rotating shaft element using timoshenko beam theory". *Journal of Mechanical Design*, Vol. 102, No. 4, pp. 793–803.

Quinz, G., Prem, M.S., Klanner, M. and Ellermann, K., 2021. "Balancing of a linear elastic rotor-bearing system with arbitrarily distributed unbalance using the numerical assembly technique". *Bulletin of the Polish Academy of Sciences: Technical Sciences*, Vol. 69, No. 6.

Saldarriaga, M.V., Steffen, V., Hagopian, J.D. and Mahfoud, J., 2010. "On the balancing of flexible rotating machines by using an inverse problem approach". *Journal of Vibration and Control*, Vol. 17, No. 7, pp. 1021–1033.

Sanches, F.D. and Pederiva, R., 2016. "Theoretical and experimental identification of the simultaneous occurrence of unbalance and shaft bow in a laval rotor". *Mechanism and Machine Theory*, Vol. 101, pp. 209–221. ISSN 0094-114X.

Sharma, A., Upadhyay, N., Kankar, P.K. and Amarnath, M., 2018. "Nonlinear dynamic investigations on rolling element bearings: A review". *Advances in Mechanical Engineering*, Vol. 10, No. 3.

Sudhakar, G. and Sekhar, A., 2011. "Identification of unbalance in a rotor bearing system". *Journal of Sound and Vibration*, Vol. 330, No. 10, pp. 2299–2313. ISSN 0022-460X. Dynamics of Vibro-Impact Systems.

Sun, X., Chen, Y. and Cui, J., 2022. "A balancing method for multi-disc flexible rotors without trial weights". *Energies*, Vol. 15, No. 14, p. 5088.

Swanson, E., Powell, C. and Weissman, S., 2005. "A practical review of rotating machinery critical speeds and modes". *Sound and Vibration*, Vol. 39, pp. 10–17.

Thearle, E.L., 1934. "Dynamic balancing of rotating machinery in the field". *Journal of Fluids Engineering*, Vol. 56, No. 8, pp. 745–753.

Thibault, N., Bourdon, A., Rémond, D. and Lecouvreur, D., 2022. "Dynamic model of a deep grooves ball bearing dedicated to the study of instantaneous angular speed of rotating assemblies". *Tribology International*, Vol. 174, p. 107753. ISSN 0301-679X.

Vance, J., Zeidan, F. and Murphy, B., 2010. *Machinery Vibration and Rotordynamics*. Wiley. ISBN 9780471462132.

Yao, J., Liu, L., Yang, F., Scarpa, F. and Gao, J., 2018. "Identification and optimization of unbalance parameters in rotor-bearing systems". *Journal of Sound and Vibration*, Vol. 431, pp. 54–69. ISSN 0022-460X.

8. RESPONSIBILITY NOTICE

The authors are solely responsible for the printed material included in this paper.